

# Test Results from a Prototype Lead Tungstate Crystal Calorimeter with Vacuum Phototriode Readout for the CMS Experiment

M.Apollonio<sup>4</sup>, G. Barber<sup>4</sup>, K.Bell<sup>6</sup>, D.Britton<sup>4</sup>, J.Brooke<sup>1</sup>, R.Brown<sup>6</sup>, J.Bourotte<sup>10</sup>, B.Camanzi<sup>2</sup>, D.Cockerill<sup>6</sup>, G. Davies<sup>4</sup>, E. Devitsin<sup>9</sup>, S.Gninenko<sup>5</sup>, N.Golubev<sup>5</sup>, Y.Goussev<sup>7</sup>, P. Grafström<sup>3</sup>, M. Haguenaue<sup>10</sup>, R.Head<sup>1</sup>, H.Heath<sup>1</sup>, P.Hobson<sup>2</sup>, A.Inyakin<sup>8</sup>, V.Katchanov<sup>8</sup>, M.Kirsanov<sup>5</sup>, L. Lintern<sup>6</sup>, A.Lodge<sup>6</sup>, E.Mcleod<sup>4</sup>, S.Nash<sup>1</sup>, D.Newbold<sup>1</sup>, M.Ukhanov<sup>8</sup>, V. Postoev<sup>5</sup>, D. Patalakha<sup>8</sup>, A. Presland<sup>1</sup>, M.Probert<sup>1</sup>, C. Seez<sup>4</sup>, I.Semeniouk<sup>5</sup>, D.Seliverstov<sup>7</sup>, B.Smith<sup>6</sup>, M.Sproston<sup>6</sup>, R.Tapper<sup>1</sup>, B.Tchuiko<sup>8</sup>

<sup>1</sup>University of Bristol, Bristol, UK, <sup>2</sup>Brunel University, Uxbridge, UK, <sup>3</sup>CERN, Geneva, Switzerland, <sup>4</sup>Imperial College, London, UK, <sup>5</sup>INR, Moscow, Russia, <sup>6</sup>CLRC, Rutherford Appleton Laboratory, Didcot, UK, <sup>7</sup>Petersburg Nuclear Physics Institute, Gatchina, Russia, <sup>8</sup>Protvino, Moscow, Russia, <sup>9</sup>P.N.Lebdev Physical Institute, Moscow, Russia, <sup>10</sup>LPNHE, Ecole Polytechnique, Palaiseau, France

## Abstract

Tests of a prototype for the Electromagnetic Calorimeter (ECAL) of the Compact Muon Solenoid Experiment (CMS) at the Large Hadron Collider are described. The basic unit for the endcap ECAL in CMS is a "supercrystal" of 25 lead tungstate crystals. Results are presented from tests of the first full-sized supercrystal in electron beams and in a 3T magnetic field. The supercrystal was exposed to electron beams with energies from 25-180GeV. An energy resolution ( $\sigma_E/E$ ) of  $(0.48 \pm 0.01)\%$  was measured at 180GeV.

PACs 07.05.Fb, 07.02.Fw

Keyword Calorimetry

Corresponding Author

Dr Helen Heath  
H.H. Wills Physics Lab  
Tyndall Ave  
Bristol  
BS8 1TL  
UK

Tel +44 117 9288725  
EMail Helen.Heath@bristol.ac.uk

# 1 Introduction

The Compact Muon Solenoid (CMS) experiment is one of two general purpose experiments to be installed at the Large Hadron Collider (LHC) proton-proton machine at CERN, Geneva. The LHC will collide opposing bunches of 7TeV protons every 25ns. The LHC environment places stringent demands on the detectors which will be installed there due to the high collision rate and radiation levels.

CMS has made precision electromagnetic calorimetry a priority and has chosen a design based on scintillating crystals of lead tungstate( $\text{PbWO}_4$ ) [1]. Lead tungstate has several properties which make it a good choice for this detector. It is intrinsically radiation hard and therefore suitable to withstand the harsh radiation environment at the LHC. Lead tungstate has a small Molière radius of 20mm, allowing separation of nearby adjacent electromagnetic showers. It has a short radiation length of 8.9mm which means that the detector can be relatively compact. Finally, by controlling the impurities, it is possible to produce crystals with a fast scintillation time of about 10ns. The CMS calorimeters are located inside a 4T superconducting solenoid magnet. A compact ECAL reduces the overall size of the magnet and of the experiment.

The CMS Electromagnetic calorimeter (ECAL) is comprised of three separate sections, the central Barrel section and two Endcaps. The Barrel covers the range of pseudorapidity  $-1.479 < \eta < 1.479$  and the two Endcaps extend the coverage of the detector to  $|\eta|=3$  with precision reconstruction of electromagnetic showers expected to  $|\eta|=2.5$ . The Barrel and Endcaps are distinguished by the details of their mechanical construction and the choice of photodetectors. In the barrel region solid state avalanche photodiodes are used to collect the scintillation light. Results from lead tungstate crystals instrumented with these devices have been reported in previous publications [2].

Avalanche photodiodes are not suitable for use in the endcap region of CMS because the radiation induced leakage currents would become excessive. The ECAL endcap uses Vacuum Phototriodes (VPTs) as photodetectors as they are radiation tolerant. The VPTs cannot be used in the barrel region as they cannot operate in the 4T transverse magnetic field.

Precision electromagnetic calorimetry is vital to the extraction of many interesting signals of new physics at the LHC. For example a low mass ( $<140\text{GeV}/c^2$ ) Higgs boson is most likely to be discovered via its decay to two high energy photons. With the kinematic cuts proposed for the final analysis [3] the range of photon energies, in the endcap, relevant to this decay is 70-500GeV.

In the CMS detector a Preshower detector will be installed in front of the ECAL Endcaps to reduce the background for photons coming from  $\pi^0$  decays. Jets where most of the energy is carried by a single  $\pi^0$  are the most important background to genuine photons. The Preshower detector consists of two layers of lead absorber, with a total thickness of  $2.8X_0$ , interleaved with two orthogonal planes of silicon strip detectors. The excellent spatial resolution of the silicon detectors improves the discrimination between single photons and closely spaced pairs of photons from the  $\pi^0$  decays, increasing the  $\pi^0$  rejection by a factor of three in the range of energies relevant to the  $H \rightarrow \gamma\gamma$  process.

The energy resolution of the ECAL in this energy range can be parameterised as

$$\frac{\sigma}{E} = \frac{a}{\sqrt{E/GeV}} \oplus \frac{\sigma_n}{E} \oplus c \quad (1)$$

where  $\sigma_n$  is the contribution from electronics noise. The stochastic term  $a$  results from photoelectron statistics contributions and the amplification noise (the ‘excess noise factor’) in the VPTs. There is also a contribution from lateral shower leakage which is estimated from Monte-Carlo to be less than  $1.4\%/\sqrt{E}$  for showers reconstructed in  $3 \times 3$  arrays of crystals. The constant term  $c$  arises from non-uniformity in the light collection along the crystal, longitudinal shower containment, intercalibration errors and absorption by inert material in the structure. At large energies the constant term becomes relatively more important and eventually dominates the resolution.

In this analysis beam events are used only if the beam particle is incident on a small area at the centre of a crystal. This means that the majority of the energy is deposited in the central crystal and so the effects of crystal-crystal intercalibration errors are small. Therefore in these tests the constant term is dominated by the longitudinal variation in light collection efficiency.

## 2 ECAL Endcap design

An important feature of the design is that all endcap crystals are the same shape and size, simplifying crystal production and detector assembly. The basic unit from which the Endcaps are constructed, the “supercrystal”, is a 5x5 array of crystals supported by a thin walled carbon fibre “alveolar” structure. A schematic drawing of a crystal and supercrystal is shown in Figure 1. The front and back faces of the crystals are square in shape and parallel to each other. As shown in Figure 1 the bottom and left hand sides meet the front and rear faces at a right angle and the other two sides are angled to produce a taper of approximately  $0.3^\circ$ . The 220mm long crystals are inserted in the alveolar in the same orientation, producing a tapered supercrystal. The supercrystals are then mounted on a backplate in such a way that they are effectively stacked on an x-y grid to form one of the two Dees which make up a complete Endcap (Figure 2). The taper provides a projective geometry with a slight offset to reduce the effect of the inter-crystal gaps.

The rigid carbon fibre alveolar unit which holds the crystals in place has twenty-five individual pockets. The internal walls of the alveolar structure are 0.4mm in thickness and the outer walls are 0.25mm. For the tests described here crystals were held in place at the front by 1cm thick aluminium endstops. In the CMS detector the endstops will be 5mm thick plastic. Between the endstops and the crystal is a layer of reflective Tyvek®<sup>1</sup>. At the back of the supercrystal metal inserts surround the VPTs and provide mechanical support. In the production supercrystals these inserts will be glued in place and provide a means of attaching the supercrystals to the Dee support plate.

In the CMS detector the crystals and associated readout will be monitored using a laser light source. The light is injected into the back of each crystal via optical fibres. These monitoring fibres are held in place by clips located in the back inserts.

## 3 The Test Setup

In 1999 the first test was made of a full-sized supercrystal. The tests were carried out in the CERN H4 beamline using electron beams with six energies in the range 25GeV to 180GeV. The supercrystal was then moved into a superconducting magnet, in the CERN H2 area, for tests in magnetic fields up to 3T. For all the tests the supercrystal was mounted in an insulated, water-cooled environmental box to stabilise the supercrystal temperature. During the beam

tests this box was mounted on a table which could move both horizontally and vertically allowing adjustment of the position of the supercrystal with respect to the beam.

### **3.1 The Supercrystal**

#### **3.1.1 The Crystals**

The twenty-five crystals used for the tests were selected from a batch of thirty, lanthanum doped, lead tungstate crystals produced at the Bogoroditsk Techno-Chemical plant in Russia. These were the first full-sized Endcap crystals – barrel crystals grown by the same producer are smaller in cross-section. Detailed measurements of the crystal optical and physical properties were performed at CERN. The mechanical dimensions were within the specified 100 $\mu$ m tolerance. The light yield for each crystal was measured using a Co<sup>60</sup> gamma source[4] and a hybrid photomultiplier(HPMT) with a bialkali photocathode which covered the rear face of the crystal.

#### **3.1.2 The VPTs**

The test array was instrumented with “1-inch” diameter VPTs, with approximately 20mm active diameter produced by three different manufacturers[5a] which were the result of extensive development work [5a,5b]. The relatively low light yield of lead tungstate, about 50 photons/MeV, means that it is essential to optimise the performance of the photodetectors. A schematic view of a VPT is shown in Figure 3. A semitransparent coating of caesium-antimony on the inner surface of the front window forms the photocathode. The anode is a fine metallic mesh; in these tests the VPTs were constructed with a variety of mesh pitches from 10-25.4 $\mu$ m. The dynode is solid metal coated with the same material as the photocathode.

An important part of the VPT development work has been to optimise their response in a magnetic field. All the VPTs had been tested before installation in the array. The tests included measurement of the gain of the devices and the photocathode efficiency in fields from 0 to 4.7T.

---

<sup>1</sup> Tyvek® is manufactured by DuPont.

During the tests the VPTs were operated with the photocathode at ground, the anode at +800V and the dynode at +600V. The signal from the anode was read out via a decoupling capacitor into a charge preamplifier with single ended drive. The 50cm signal cable between the VPTs and the preamplifier is the expected length of cable in the CMS configuration. In the testbeam the preamplifiers are readout via ~80m cables connected to a charge integrating LeCroy 1881 ADC with a 200ns integration gate. The gate length for these tests was determined by the shaping time of the preamplifiers.

### **3.2 The Mechanical Structure**

Figure 4 is a photograph of the supercrystal installed in the environmental box, with most of the elements of the mechanical structure visible. The supercrystal was encased in a structure for mechanical support and to allow it to be easily transported. This support consists of an aluminium baseplate on which the supercrystal rests, an aluminium case which surrounds the sides of the supercrystal and a carrying handle. One of the trapezoidal pieces of metal which form part of the handle can be seen clearly in the photograph. These two pieces are joined at the top by a beam to which is attached a metal eye so that the supercrystal can be craned in and out of the environmental box.

Tests of the ECAL prototype with a prototype preshower detector are described elsewhere [6]. To allow these tests to take place, the supercrystal rested on rails enabling it to roll forward. The Preshower prototype was mounted on the front of the environmental box. The forward repositioning of the supercrystal allowed a more realistic configuration of these two detectors. In this configuration optical fibres carrying LED light to the front of the crystals, for monitoring, had to be removed.

The back of the supercrystal butts up against a 5cm thick aluminium backplate. A hole in the centre of the backplate allows the VPT cables to reach the electronics boxes which are mounted on a support plate separated from the backplate by insulating pillars. A water cooled copper plate was attached to the rear of the electronics box.

The scintillation yield of lead tungstate depends on temperature with a change of  $-1.9\%/^{\circ}\text{C}$  at room temperature; hence the need for an insulated environmental box. The box was cooled by water which circulated through a system of copper pipes welded to the box walls. The temperature in the environmental box was monitored by 15 temperature probes

distributed throughout the box. Figure 5 shows the results from two of these probes situated on the supercrystal and support structure. The temperature probes were used to measure changes in the temperature since any change in temperature will affect the light yield. No absolute calibration of the probes was performed. The temperature shows a diurnal variation with a peak to peak variation of about 0.1°C.

### **3.3 Monitoring**

The performance of the supercrystal was monitored using pulsed light emitting diodes with a peak spectral emission of 470nm. Light from the pulsers was injected into two fibre bundles. One fibre bundle was used to illuminate all the crystals from the front and one bundle to illuminate them from the rear. In the CMS configuration and in the tests with the preshower in place, light injection was only possible from the rear of the crystals. In addition a charge injection system was used to inject a known charge into the front end of the preamplifiers. LED and charge injection events were recorded during all the data taking runs. During all runs the noise, both within the beam spill and outside, was continuously monitored by taking random “pedestal” triggers.

## **4 Beam Tests**

### **4.1 Calibration Runs**

The supercrystal was calibrated using a 50GeV electron beam. The table was adjusted so that the beam was directed into each crystal in turn. A sample of 40,000 events was collected in each crystal. The calibration procedure was repeated at regular intervals throughout the data taking period.

To determine the calibration constants the response of a selected crystal to the beam was plotted as a function of the lateral position of incidence of the electron. Such a plot is shown in Figure 6 for the central crystal. The effective centre of the crystal was then determined from this plot by selecting the x co-ordinate corresponding to the maximum response. This procedure was repeated for the y co-ordinate. The response of the crystal to beam electrons falling within the central 4x4mm<sup>2</sup> was plotted. It was expected from Monte-Carlo studies that about 80% of the beam energy would be deposited in the crystal into which the beam was directed. Using a Gaussian fit to the single crystal response plot the

conversion factor from ADC counts to GeV was calculated. Finally the distribution of the sum of the energy in the central nine crystals was plotted (figure 7). A further normalisation factor was applied to all calibration constants such that a Gaussian fit to the energy distribution in figure 7 had a mean value of 50GeV.

## 4.2 Energy Scans

In order to study the various contributions to the energy resolution it was necessary to measure the resolution at several beam energies. Rearranging Equation 1 yields

$$\left( \frac{\sigma^2 - \sigma_n^2}{E^2} \right) = \frac{a^2}{E / GeV} + c^2 \quad (2)$$

The values of  $\sigma$  and  $\sigma_n$  are determined from fits to the data.  $E$  is the incoming beam energy. Beams of energy 25, 35, 50, 80, 120 and 180 GeV were directed into the centre of each of the central nine crystals and 100,000 events taken at each beam energy. For each run the crystal into which the beam was directed was taken as the centre of a square of nine crystals. The sum of the energy in these nine crystals was calculated and plotted – using only those events where the incident electron falls within the central 4x4mm<sup>2</sup> of the 3x3 crystals. A Gaussian fit to the energy sum distribution was used to determine the resolution,  $\sigma$ . The value of  $\sigma_n$  for in-spill pedestal triggers was determined by fitting the distribution of the linear sum of the energy seen in the nine crystals.

Figure 8 shows the results of the energy scan runs with the beam directed into crystal 18. The fitted results for the stochastic and constant terms are given in table 1. The average energy equivalent of the noise per channel is 122MeV.

## 4.3 Magnet Field Scans

The VPTs used in these tests were produced as part of the research and development exercise which aimed to optimise the properties for application in CMS including minimising the dependence of the VPT response on the magnetic field. As part of the test program the supercrystal was installed in a 3T superconducting magnet located in the H2 area at CERN. Data were taken using the LED monitoring system at sixteen values of the magnetic field from 0-3T. The response of the VPTs depends on the magnetic field and on the angle of the VPT axis to the field. In CMS the VPTs will have to function in a 4T field and at angles of up to 25° to that field. Figure 9 shows the response of the VPTs as a

function of magnetic field for the different VPTs where the VPT axes are at  $15^\circ$  to the magnetic field. Following an initial steep fall in the response a plateau is reached and the VPT response varies only slowly with magnetic field.

## 5 Discussion

The design goals for the energy resolution of the combined crystal Endcap and preshower detector are a total stochastic term  $5.7\%/\sqrt{E/GeV}$ , constant term 0.55% and electronics noise term of 150MeV per channel [7]. This resolution yields a signal significance of greater than 5 for the entire range of Higgs masses where the decay  $H \rightarrow \gamma\gamma$  is the most likely discovery channel. Signal significance is defined as  $N_s/\sqrt{N_B}$  where  $N_s$  is the number of signal events and  $N_B$  is the number of background events. The noise performance achieved in these tests was 122MeV per channel, although the electronics used is very different from the final system.

Table 2 summarises the various contributions to the energy resolution in design goals and in the testbeam setup. These contributions are discussed in more detail below.

### 5.1 Constant Term

The constant term becomes increasingly significant with increased particle energy and so it is important that this term is well controlled. Contributions to the measured constant term can come from several sources; longitudinal shower containment, beam momentum spread, calibration errors and the longitudinal non-uniformity of the crystal response.

The efficiency with which light reaches the photodetector depends on the distance it has to travel within the crystal. Non-uniformity in the light collection efficiency is due to two effects, crystal absorption and the focussing effect of the crystal taper. If the intrinsic non-uniformity is too large then it must be reduced in order to obtain a small constant term. Possible methods for improving the collection uniformity include grinding one or more sides of the crystals or painting a pattern of dots on the crystal surface. These procedures not only increase the manufacturing time but also reduce the overall light collection efficiency thus increasing the stochastic and noise terms.

The overall goal for the constant term of 0.55% includes supercrystal intercalibration errors in addition to the contribution from the non-uniformity of light collection and other sources. The goal for the contribution from non-uniformity due to the crystals alone is 0.3%.

From Monte-Carlo studies the limited longitudinal shower containment is expected to contribute 0.15% to the constant term. The contribution due to the beam momentum spread at the H4 beamline is estimated to be 0.08%. During these tests the beam is directed into a small area in the centre of the central crystal and more than 80% of the energy is deposited within the crystal, the results are therefore insensitive to crystal to crystal intercalibration errors. In these tests the average measured constant term is  $(0.29 \pm 0.06)\%$ . Taking the above factors into account the intrinsic contributions from non-uniformity of light collection are estimated to be 0.23% to be compared with the goal of  $<0.3\%$ .

## 5.2 Stochastic Term

The stated design goal for the stochastic term[7] of  $5.7\%/\sqrt{E/GeV}$  includes an estimated contribution<sup>2</sup> from the Preshower detector of  $5\%/\sqrt{E/GeV}$ . Subtracting the Preshower contribution from the overall design goal leaves a goal of  $\sqrt{5.7^2 - 5.0^2}\%/\sqrt{E/GeV} = 2.7\%/\sqrt{E/GeV}$  for the photostatistics contribution.

Both the measured stochastic term and the design goal include contributions from lateral shower containment, determined to be less than  $1.4\%/\sqrt{E/GeV}$  using Monte-Carlo studies[6]. The average photostatistics contribution measured in these tests is therefore  $\sqrt{4.1^2 - 1.4^2}\%/\sqrt{E/GeV} = 3.6\%/\sqrt{E/GeV}$  which must be compared with the design goal for this term of  $2.7\%/\sqrt{E/GeV}$ . In the CMS setup this term may increase slightly due to an estimated 20% reduction in VPT response in a 4T magnetic field.

---

<sup>2</sup> In fact the Preshower contribution is not well described by this term. The presence of the Lead absorber degrades the performance of the calorimeter but the information used from the silicon detectors can be used to partially recover the performance[6].

## 6 Conclusions

A prototype supercrystal for the CMS Endcap electromagnetic calorimeter has been built and tested at CERN in electron beams and in magnetic fields. The results obtained have been compared with the design goals stated in the CMS ECAL Technical Design Report(TDR)[7]. The contributions to the overall resolution of photostatistics and crystal non-uniformity are determined to be  $(3.6 \pm 0.9)\% / \sqrt{E / GeV}$  and  $(0.26 \pm 0.05)\%$  respectively compared with the design goals of  $2.7\% / (\sqrt{E / GeV})$  and  $0.3\%$ . These results have been achieved with prototype crystals which were larger than any previously produced.

The overall resolution obtained here is not directly comparable with the design goal for the CMS detector. However if the design goal parameters are used to calculate the expected energy resolution for 180GeV electrons the value obtained is  $\sigma/E = 0.47\%$ . This figure may be compared with the measured resolution  $\sigma/E = (0.48 \pm 0.01)\%$ .

## References

- [1] CMS Collaboration (G.L.Bayatian et al.), CERN/LHCC 94-38
- [2] E. Auffray et.al. Nucl. Instr. and Meth A 412 (1998) 223
- [3] M. Pimiä et. al. CERN 90-10, vol III (1990) 547
- [4] G.J.Davies et.al. CMS Note 1999/022
- [5a] K.W.Bell at.al. Nucl. Instr. and Meth A 469 (2001) 29
- [5b] N.A.Bajanov et. al. Nucl. Instr. and Meth A 442 (2000) 146
- [6] P.Aspell et.al. CMS Note 2000/001.
- [7] CMS Collaboration (G.L.Bayatian et al.), CERN/LHCC 97-33

Table 1 Values of the stochastic term  $a$  and the constant term  $c$ , in the equation  $\sigma/E = a/\sqrt{E} \oplus \sigma_n/E \oplus c$  obtained from fits to the experimental data. The width  $\sigma$  was measured by making a sum of the energy in the 3x3 crystal array centred on the crystal into which the beam was directed. The noise term  $\sigma_n$  was measured directly from pedestal events.

Central Crystal	Stochastic Term $a$ (%)	Constant Term $c$ (%)
7	2.9±0.4	0.41±0.02
8	2.5±0.6	0.31±0.03
9	4.6±0.5	0.27±0.07
12	4.5±0.2	0.25±0.04
13	4.2±0.4	0.23±0.05
14	5.5±0.6	0.31±0.08
17	4.5±0.4	0.28±0.05
18	3.3±0.3	0.35±0.04
19	4.7±0.4	0.23±0.06
Average	4.1±1.0	0.29±0.06

Table 2 The contributions to the energy resolution which contribute to the CMS design goals and to the testbeam set up. The energy design goal energy resolutions at 50 and 180GeV include the beam momentum spread but not the preshower term or the intercalibration error – allowing a direct comparison between the measured and calculated values.

		Design Goal from [7]	Testbeam
Contributions to the Stochastic term			
	Preshower term	$5.0\% / \sqrt{E / GeV}$	N/A
	Lateral Shower Containment	$1.4\% / \sqrt{E / GeV}$	$1.4\% / \sqrt{E / GeV}$
	Photostatistics	$2.7\% / \sqrt{E / GeV}$	$3.6\% / \sqrt{E / GeV}$
Total Stochastic Term		$5.7\% / \sqrt{E / GeV}$	$(4.1 \pm 1.0)\% / \sqrt{E / GeV}$  Measured Value
Contributions to the Constant term			
	Intercalibration Errors	0.4%	N/A
	Longitudinal Shower Containment	0.1%	0.15%
	Beam Momentum Spread	N/A	0.08%
	Crystal non-uniformity	<0.3%	0.23%
Total Constant Term		0.55%	$(0.29 \pm .06)\%$  Measured Value
Noise		150MeV/channel	122MeV/channel  Measured Value
$\sigma/E$ at 50GeV	The design goal numbers are derived by considering all contributions relevant to the test beam setup in order to compare directly to the measured values.	1.05%	$(1.17 \pm 0.03)\%$  Measured Value
$\sigma/E$ at 180GeV		0.47%	$(0.48 \pm 0.01)\%$  Measured Value

Figure 1

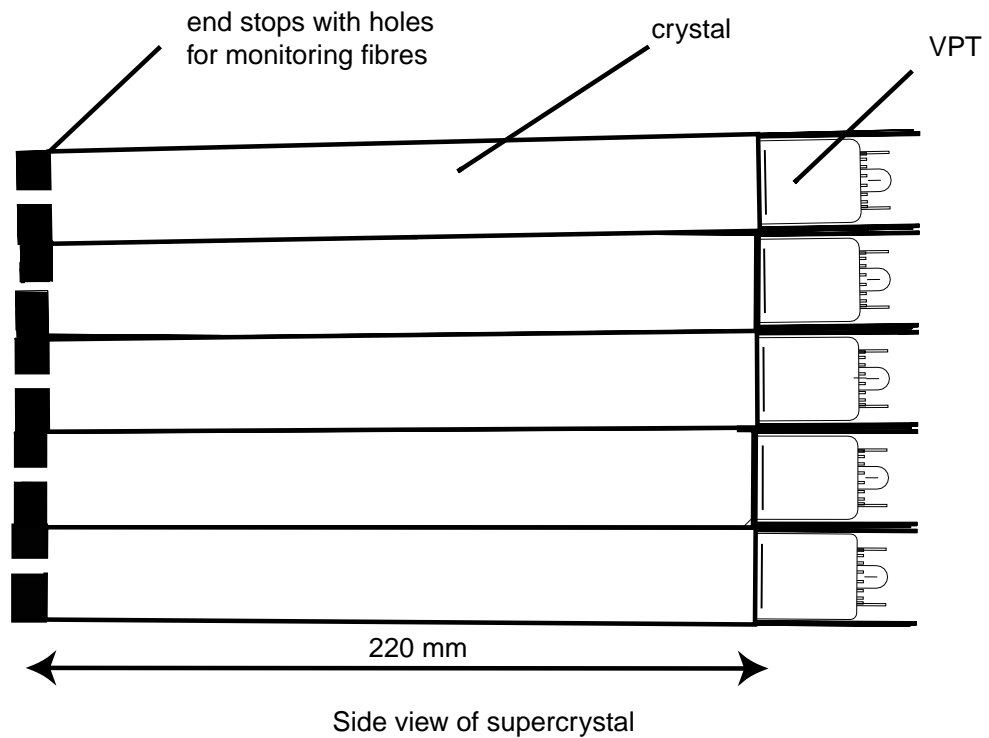
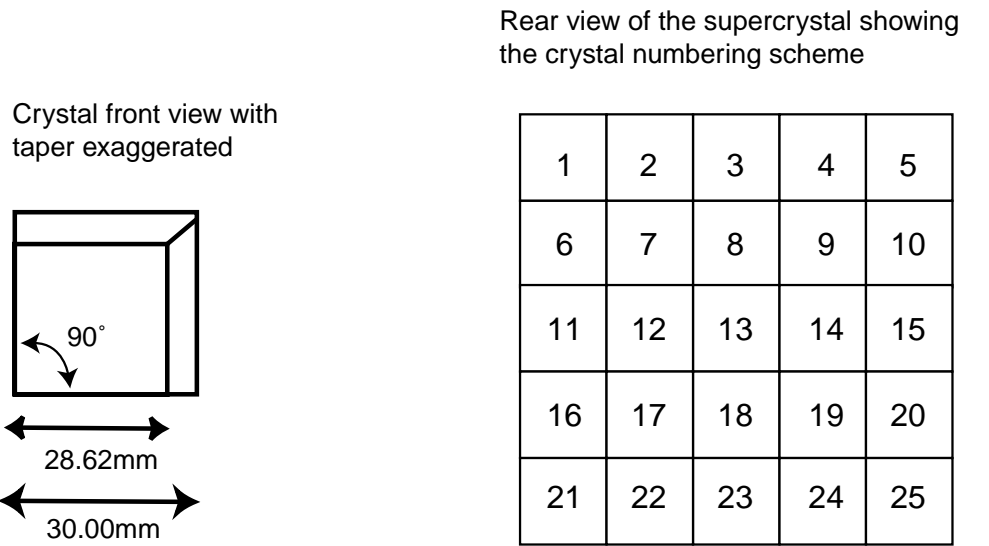




Figure 2

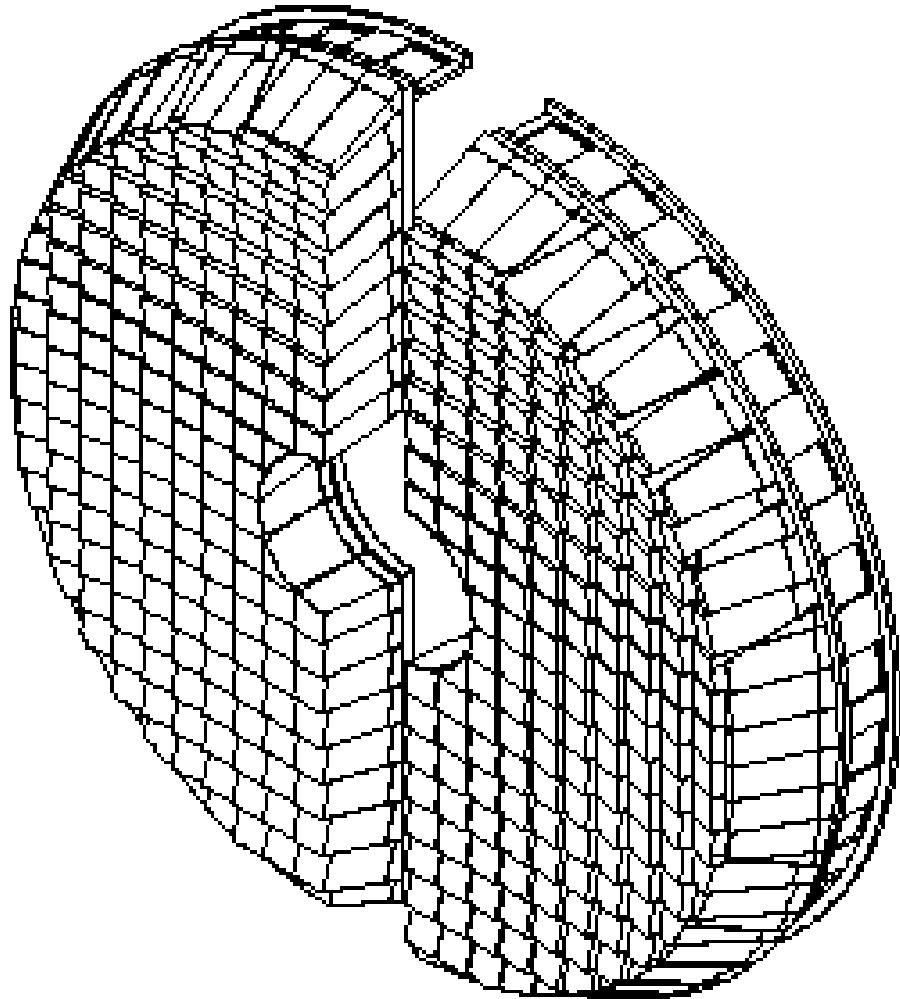


Figure 3.

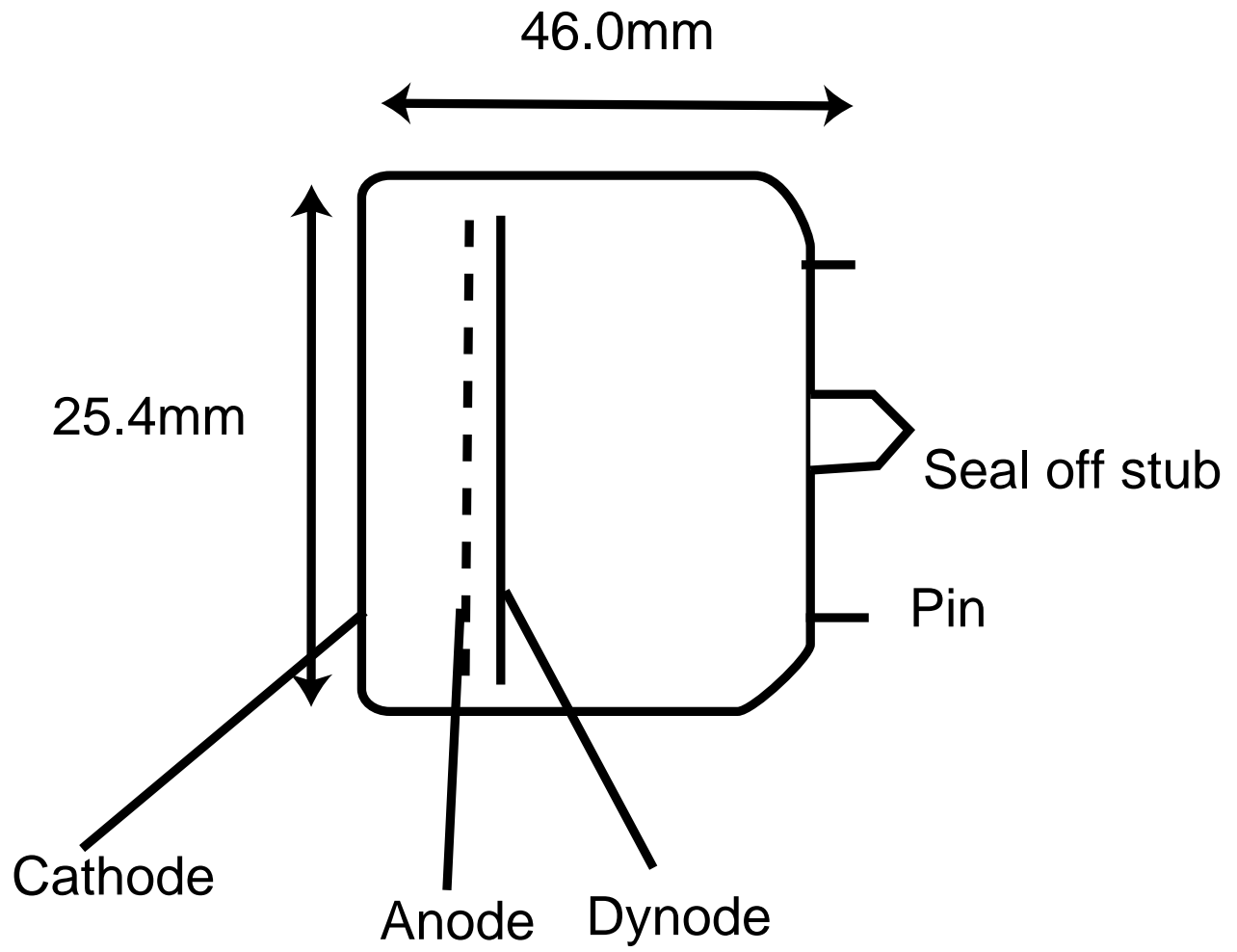


Figure 4

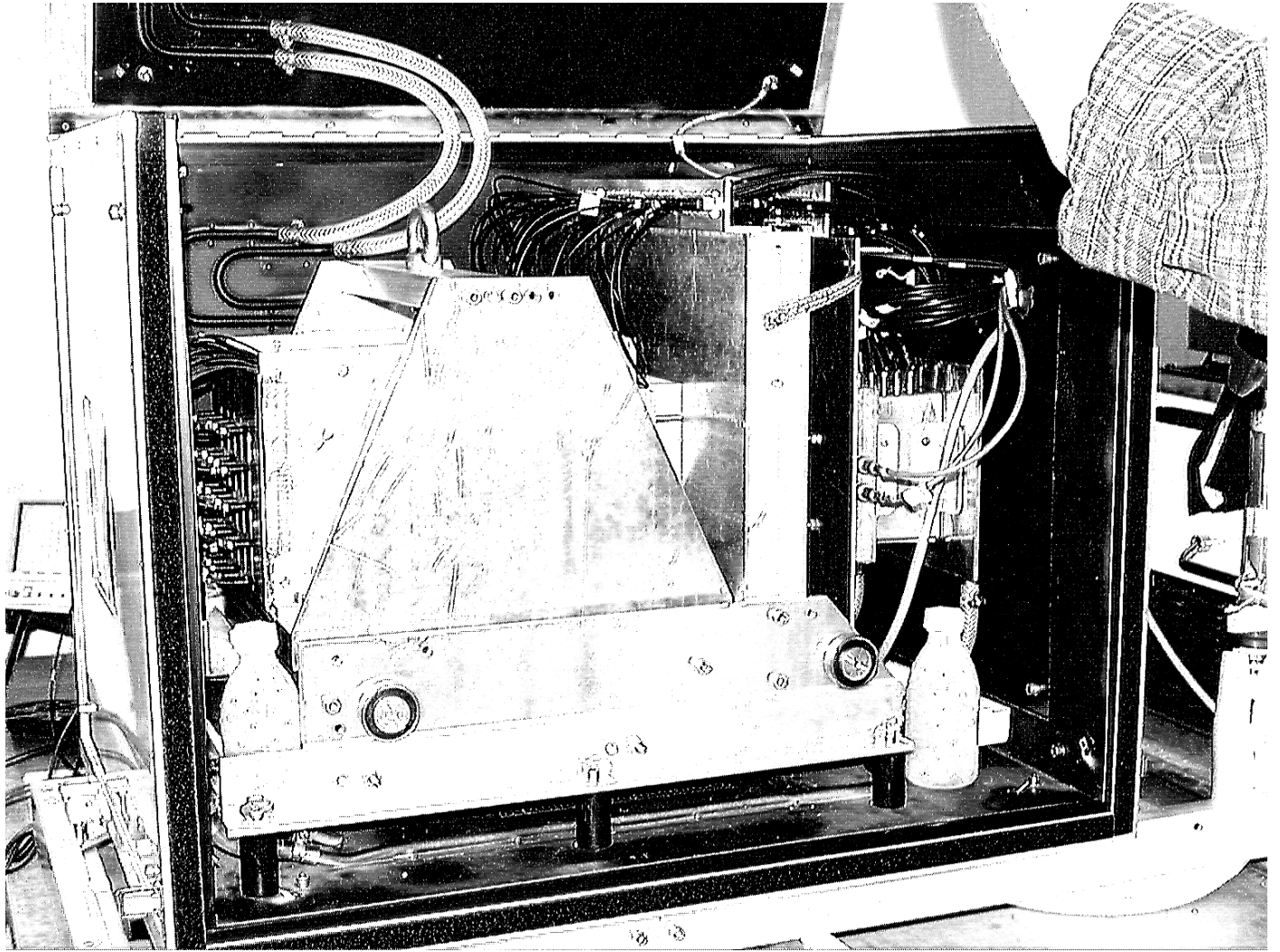


Figure 5

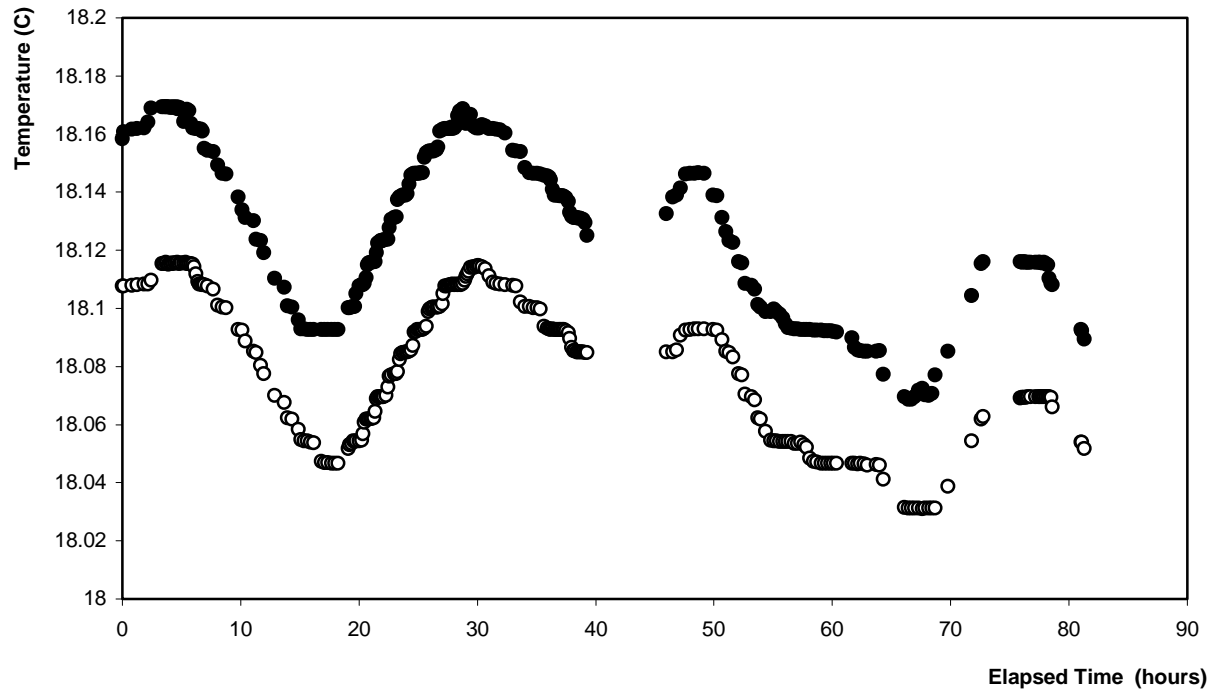


Figure 6

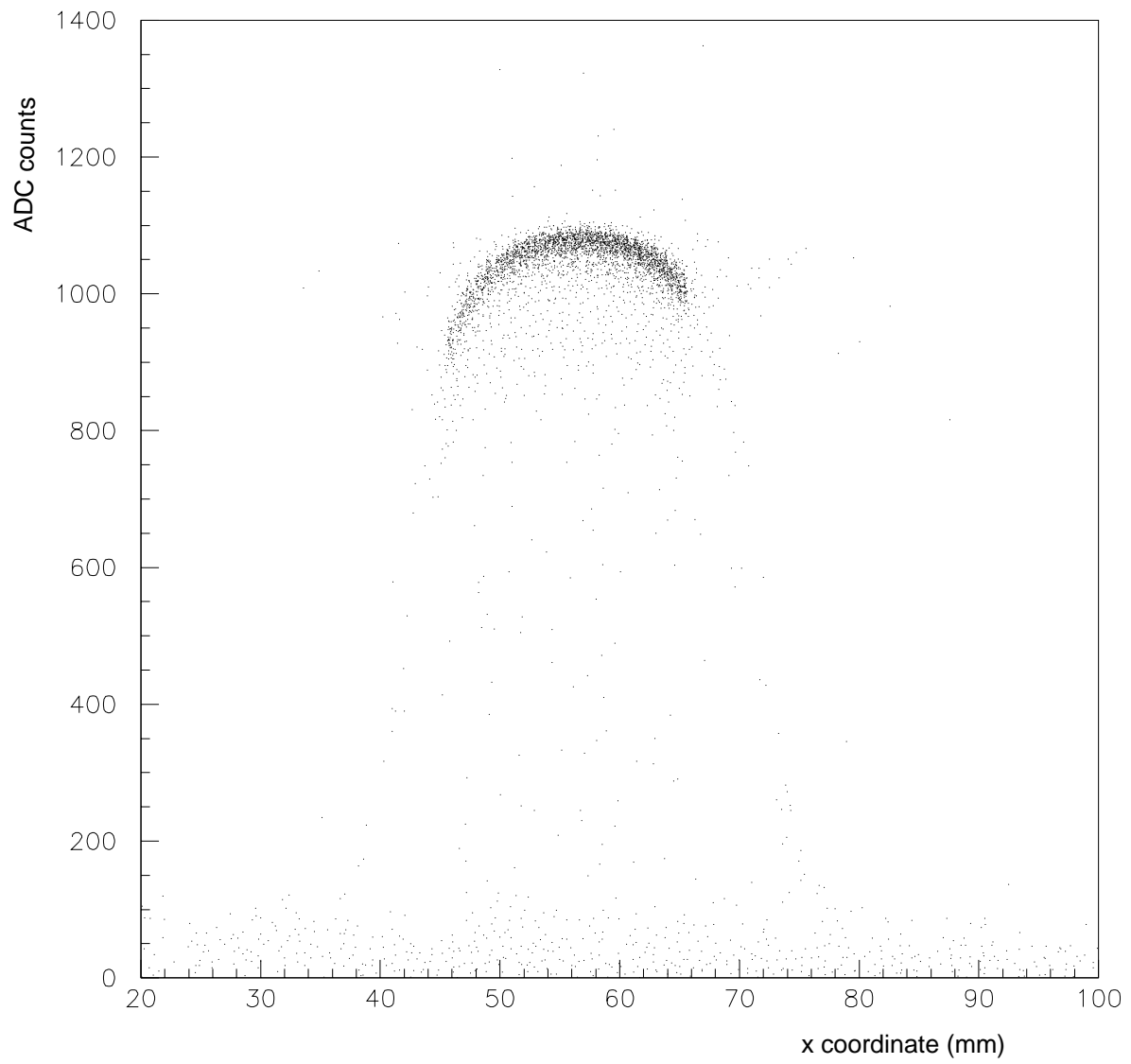


Figure 7

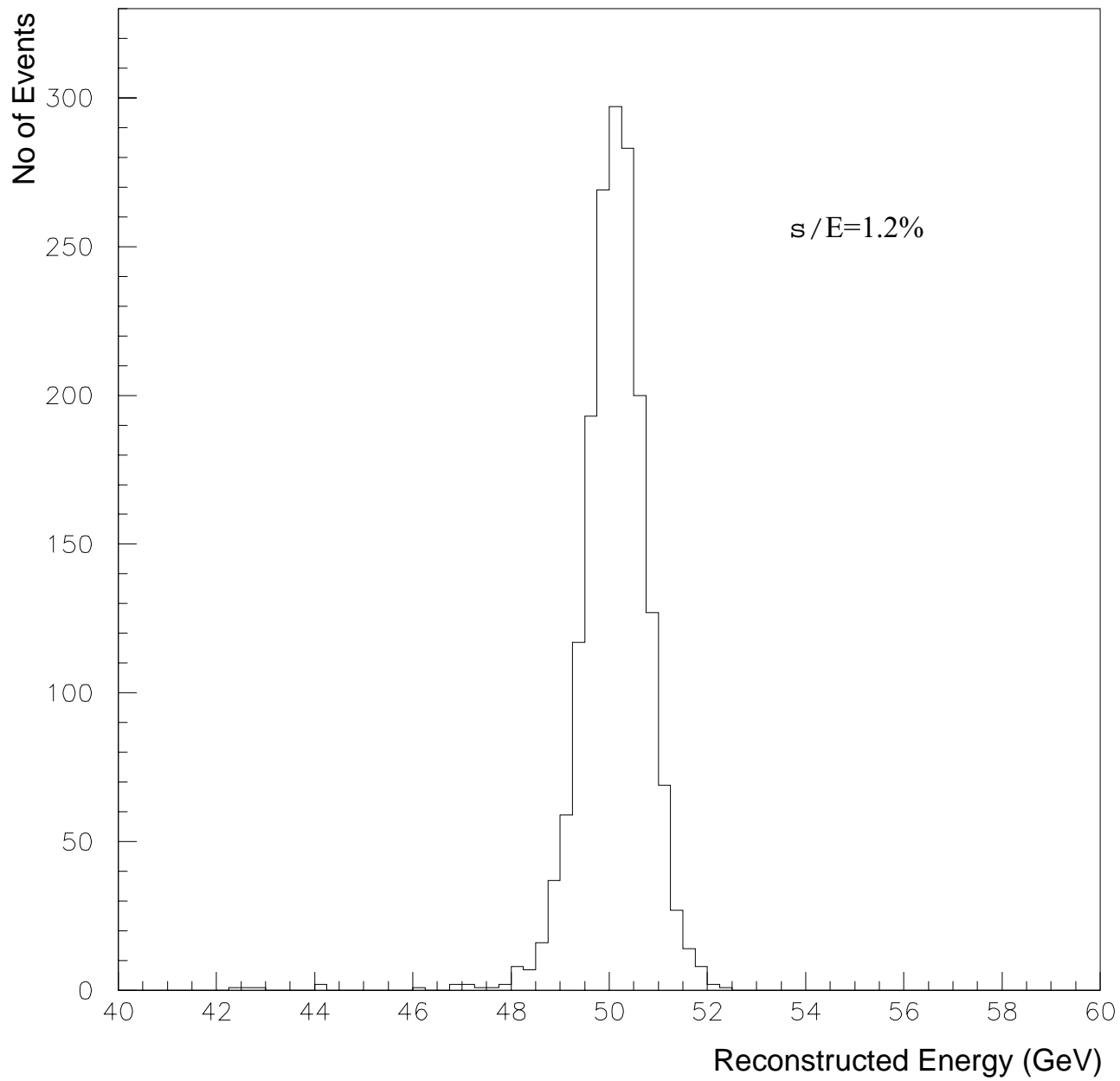


Figure 8

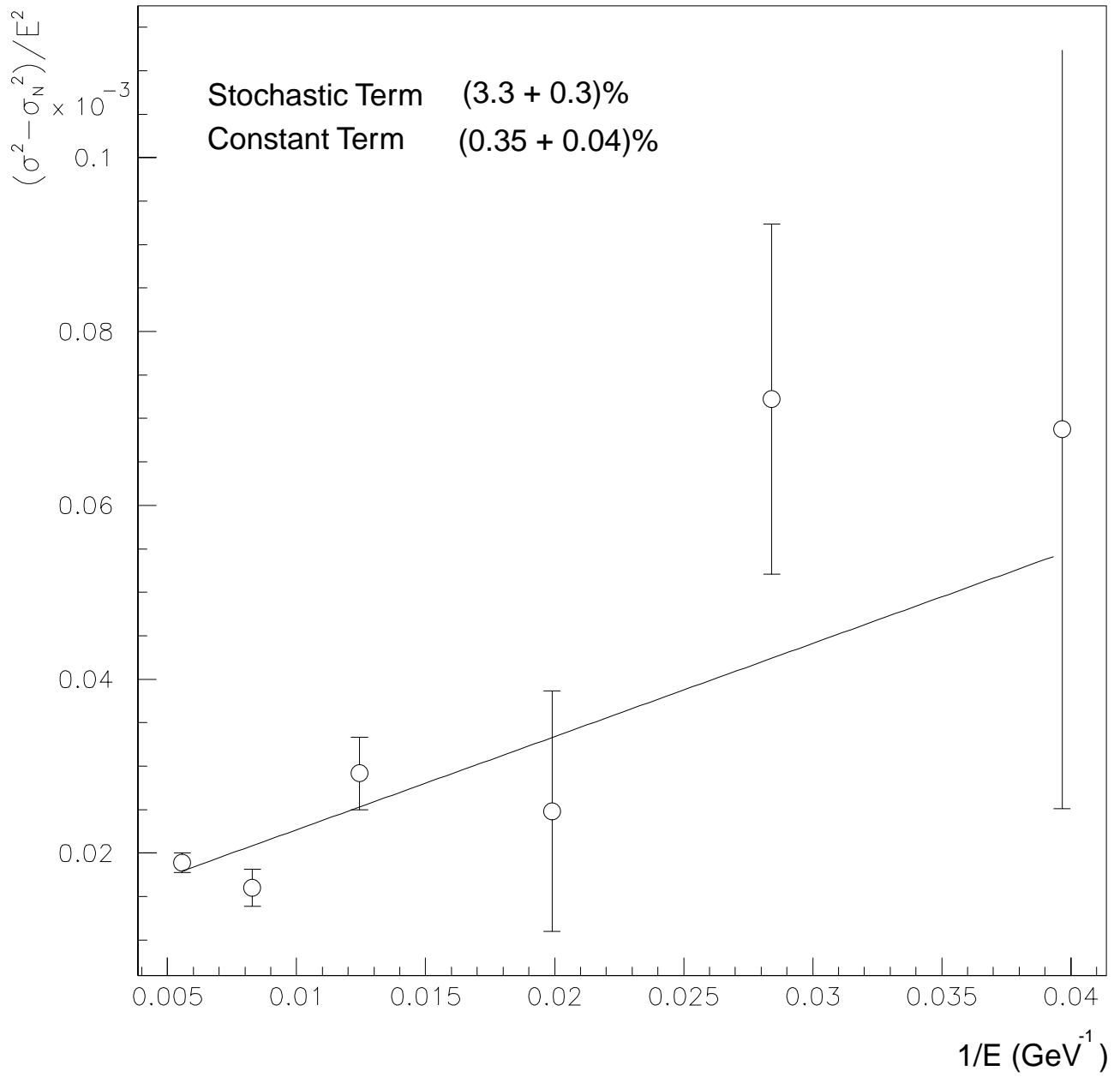


Figure 9

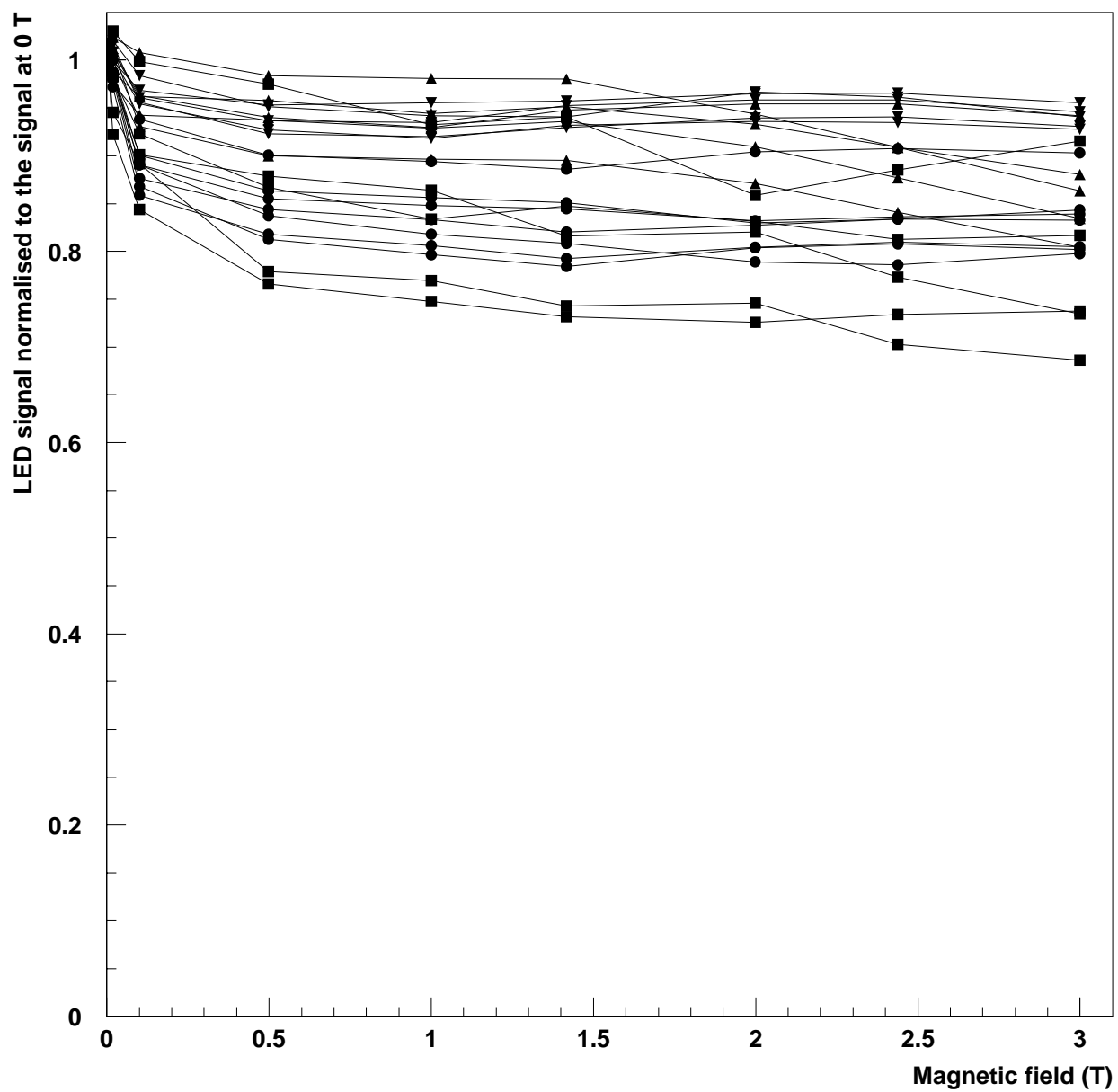


Figure 1 Schematic views of a crystal and the supercrystal.

Figure 2 The arrangement of supercrystals to form two Dees which together form a complete Endcap. The supercrystals are mounted on a metal backplate. Partial supercrystals are shown at the inner and outer edges.

Figure 3 Schematic view of a VPT showing the solid dynode and the mesh anode. The cathode is formed from a coating of caesium-antimony on the inner surface of the front window.

Figure 4 The Supercrystal in the environmental box prior to the tests. The beam enters from the left hand side. In this picture the supercrystal is rolled backwards and the front monitoring fibres are present. To the right of the picture the 5cm thick backplate can be seen and behind it the boxes containing the electronics

Figure 5 Variation of temperature with elapsed time during the data taking runs. The temperature was monitored with fifteen probes distributed throughout the environmental box. The plot shows results from two of these probes. A diurnal variation can be seen in the temperature with a peak to peak change of about  $0.1^{\circ}\text{C}$

Figure 6 The signal, in ADC counts, from crystal 13 with a 50GeV electron beam plotted as a function of beam position in x as measured by the beam chambers. The signal decreases as the beam nears the edges of the crystal and more of the shower falls in neighbouring crystals.

Figure 7 The total energy seen in the nine central crystals of the array with a 50GeV electron beam directed into the central crystal. The quoted value for  $\sigma/E$  was determined from a Gaussian fit to the data.

Figure 8  $(\sigma^2 - \sigma_N^2)/E^2$  as a function of  $1/E$  for crystal 18. The straight line is a fit to the data and has been used to determine the stochastic term ( $a$ ) and the constant term ( $c$ ) in equation 2.

Figure 9 The signal seen in each channel when the LED is pulsed versus the magnetic field. The signals are normalised to the signal at 0T. In these test the VPTs were oriented at  $15^\circ$  to the magnetic field. Different symbols represent VPTs from different manufacturers.